Coupling between Structural and Dielectric Relaxations of Methanol and Ethanol Studied by Molecular Dynamics Simulation

Journal:	*The Journal of Physical Chemistry*
Manuscript ID	jp-2020-056857.R1
Manuscript Type:	Article
Date Submitted by the Author:	n/a
Complete List of Authors:	Yamaguchi, Tsuyoshi; Nagoya Daigaku Kogakubu Daigakuin Kogaku Kenkyuka, Department of Materials Process Engineering

Coupling between Structural and Dielectric Relaxations of Methanol and Ethanol Studied by Molecular Dynamics Simulation

*Tsuyoshi Yamaguchi**

Graduate School of Engineering, Nagoya University, Chikusa, Nagoya, 464–8603, Japan

Tel: +81-52-789-3592

E-mail: yamaguchi.tsuyoshi@material.nagoya-u.ac.jp

ABSTRACT

The microscopic origin of the fast dielectric relaxation modes and the integrated dielectric relaxation times of methanol and ethanol was investigated by means of cross correlation analysis of molecular dynamics simulation. Random force on the fluctuation of collective dipole moment was correlated with the two-body density mode in both real and reciprocal spaces. A strong coupling was observed with the OH alternation mode at 30 nm^{-1}, suggesting that alternating switching of the hydrogen bond within a hydrogen-bonding chain is the principal origin of the retarded friction on the collective dipole moment. The relaxation of the coupling was much slower than that of the partial intermediate scattering functions at the corresponding wavenumber, which suggests the breakdown of the factorization approximation employed in the mode-coupling theory. Although prepeak structure is strongly coupled to the viscoelastic relaxation, its coupling with the dielectric relaxation is relatively weak. The difference between the viscoelastic and the dielectric relaxations was discussed in terms of the different symmetries of the shear stress tensor and the collective dipole moment.

1. INTRODUCTION

Monoalcohol is one of the famous classes of organic solvents. It plays important roles in various fields of industry, and it is indispensable to our daily life. Nonetheless, there remain many unresolved questions on the fundamental physicochemical properties of monoalcohols and their microscopic bases. [1, 2] Monoalcohol is characterized by an OH group in a molecule, which interacts with other alcohol molecules through the intermolecular hydrogen bond. Although it is needless to say that the hydrogen bond plays essential roles in various properties of liquid monoalcohols, the understandings on how the roles are actually played is yet unsatisfactory at present. The current achievements and the remaining questions were summarized in an excellent review published by Böhmer and coworkers in 2014. [1]

Dielectric relaxation is an important dynamic property of liquid monoalcohols that has been attracting many researchers. [1-7] Dielectric relaxation is the reorientational relaxation of collective dipole moment. It is defined as the linear response of the collective dipole moment to the external electric field, and it is related to the equilibrium time correlation function of the collective dipole moment by the linear response theory. [8, 9]

The dielectric relaxation of small 1-alcohols, such as methanol and ethanol, is characterized by the strong principal relaxation and adjacent high-frequency processes. [3] The slowest relaxation is reproduced well by a Debye function. On the high-frequency side of the Debye relaxation, weak additional relaxations are observed, and they are usually approximated as the sum of two Debye functions. The relaxation time of the slowest Debye mode is long compared with the expectation based on the molecular size and the shear viscosity. For example, the dielectric relaxation time of methanol is 52 ps at 298 K, [3] which is more than an order of magnitude longer than that of acetonitrile, 3.3

ps,[10] although their molar volumes, shear viscosities and dielectric constants are close to each other (40.7 cm^3/mol, 0.55 mPa s, and 32.7 for methanol, and 52.9 cm^3/mol, 0.34 mPa s, and 35.9 for acetonitrile at 298 K, respectively). [11] Davidson and Cole pointed out already in 1951 that the hydrodynamic volume of 1-propanol calculated from the dielectric relaxation time and shear viscosity is 1000 times larger than those of glycerin and propylene glycol.[12] A question on the dielectric relaxation of 1-alcohols is thus why the principal dielectric relaxation is so slow.

The comparison of the dielectric relaxation spectra with other collective dynamics has also been performed by many researchers. [1] Although the slowest Debye mode is hardly observed in other relaxation spectra, the time scales of the high-frequency processes in the dielectric relaxation are comparable to those of other collective dynamic modes. Detailed comparison with the depolarized light scattering spectrum was performed on liquid methanol [4] and 1-propanol, [13] in which the relaxation modes in the depolarized light scattering spectrum were related to the high-frequency modes of the dielectric relaxation.

Viscoelastic relaxation is another target for the comparison with the dielectric relaxation spectrum. The frequency-dependent shear viscosity of *n*-alcohols can be measured at the ambient condition by means of transverse ultrasonic technique.[14, 15] Since many monoalcohols are easily supercooled, conventional mechanical rheometer can also be applied to deeply supercooled state. Jacobsen and coworkers measured the dielectric and viscoelastic spectra of supercooled 2-ethyl-1-hexanol and 2-butanol at various temperatures near the glass transition, and demonstrated that the time scale of the viscoelastic relaxation is close to that of the high-frequency dielectric process.[16]

The fluctuation of the heterogeneous structure is another dynamic mode whose relation with the dielectric relaxation is interesting. 1-alcohols can be regarded as ones of the simplest amphiphilic molecules, because they possess both hydrophilic OH and hydrophobic alkyl groups. In neat liquid phase of the 1-alcohols, the OH groups interact with each other strongly to form linear hydrogen-bonding chain. The alkyl groups expelled by the hydrogen-bonding chain also tend to cluster. As a result, the structure of neat liquid 1-alcohols is heterogeneous, composed of polar OH and nonpolar alkyl domains.

The heterogeneity of the liquid structure of 1-alcohol appears as the prepeak of the X-ray structure factor. [1, 17-19] In addition to the strong main peak at q = 15 – 20 nm^{-1}, reflecting the contact distance between the alkyl groups, liquid 1-alcohols exhibit a peak called "prepeak" in the lower-q region. The position of the prepeak shifts to lower-q with increasing the length of the alkyl chain.[17] Computer simulation studies revealed that the prepeak originates mainly from the correlation between O-atoms,[18] and the peak position reflects the distance between different hydrogen-bonding chains. Similar prepeaks have also been reported in room-temperature ionic liquids [20, 21] and concentrated electrolyte solutions.[22, 23]

The dynamics of the heterogeneous structure can be determined experimentally from the neutron or X-ray intermediate scattering functions at the prepeak. [24-28] Sillrén and coworkers measured the neutron intermediate scattering functions of supercooled 1-propanol at both prepeak and main peak as functions of temperature.[24] Compared with the dielectric relaxation, the relaxation times of both peaks are shorter than that of the slowest Debye mode, and they are close to that of the high-frequency process. Since the

viscoelastic relaxation time is close to the relaxation time of the high-frequency dielectric process, it is also close to that of the intermediate scattering functions.

In a series of our previous works, we investigated both experimentally and computationally how the presence of the prepeak structure affects the shear viscosity and viscoelastic relaxation of liquid 1-alcohols. From the comparison with the viscoelastic relaxation separately determined experimentally, the viscoelastic relaxation time matched with the prediction from the relaxation of the intermediate scattering function at the prepeak, suggesting that the slowest mode of the viscoelastic relaxation originates from the dynamics of the heterogeneous structure.[27] Similar coincidence was also observed in our molecular dynamics (MD) simulation.[29] Furthermore, we evaluated the coupling between the prepeak structure and shear stress directly using MD simulation, and found the strong coupling between them.[30]

Based on the correspondence between the relaxation time of the high-frequency dielectric process and that of the viscoelastic relaxation, one may consider that the former is also coupled to the dynamics of the prepeak structure. In order to examine this idea, however, we need to treat the coupling between the dielectric relaxation and the prepeak structure in a similar way to that of the viscoelastic relaxation.

In this work, we extend the cross correlation analysis we have employed to clarify the coupling between the viscoelastic and structural relaxations to the dielectric relaxation, and apply the formalism to liquid methanol and ethanol. First, the generalized Langevin theory is applied to the collective dipole moment, and the memory function for the dielectric relaxation is deduced. Then, the random force on the collective dipole moment is correlated with the two-body density to extract the coupling between the friction on the dipole moment and the structural relaxation. Since the memory function of finite

relaxation time corresponds to the deviation of the dielectric relaxation from the Debye function, the structural relaxation extracted in this analysis can be interpreted as the microscopic origin of the high-frequency dielectric processes.

2. THEORY

According to the generalized Langevin theory, the dynamics of the collective dipole moment, $\boldsymbol{\mu}(t)$, is described as[8, 31, 32]

$$\frac{1}{\Omega_0^2}\ddot{\boldsymbol{\mu}}(t) = -\int_0^t d\tau \Gamma_\mu(t-\tau)\dot{\boldsymbol{\mu}}(\tau) - \boldsymbol{\mu}(t) + \boldsymbol{R}_\mu(t), \quad (1)$$

where $\boldsymbol{\mu}(t)$ and $\dot{\boldsymbol{\mu}}(t)$ are chosen as the set of the variables explicitly considered in the generalized Langevin theory. The characteristic frequency, Ω_0, is related to the instantaneous correlation of $\boldsymbol{\mu}(t)$ as

$$\Omega_0^2 \equiv \frac{\langle|\dot{\boldsymbol{\mu}}|^2\rangle}{\langle|\boldsymbol{\mu}|^2\rangle}. \quad (2)$$

The memory function, $\Gamma_\mu(t)$, is related to the time correlation function of the random force, $\boldsymbol{R}_\mu(t)$, as

$$\Gamma_\mu(t) = \frac{\langle \boldsymbol{R}_\mu(0)\cdot\boldsymbol{R}_\mu(t)\rangle}{\langle|\boldsymbol{\mu}|^2\rangle}. \quad (3)$$

The time development of the normalized time correlation function of $\boldsymbol{\mu}(t)$, defined as

$$C_\mu(t) \equiv \frac{\langle \boldsymbol{\mu}(0)\cdot\boldsymbol{\mu}(t)\rangle}{\langle|\boldsymbol{\mu}|^2\rangle} \quad (4)$$

is then given by

$$\frac{1}{\Omega_0^2}\ddot{C}_\mu(t) + \int_0^t d\tau \Gamma_\mu(t-\tau)\dot{C}_\mu(\tau) + C_\mu(t) = 0. \quad (5)$$

Using eq. (5), $\Gamma_\mu(t)$ can be calculated numerically from $C_\mu(t)$ obtained by MD simulation. The integrated relaxation time, τ_μ, is related to the time integral of the memory function as

$$\tau_\mu \equiv \int_0^\infty C_\mu(t)dt = \int_0^\infty \Gamma_\mu(t)dt. \quad (6)$$

When the relaxation of the memory function is instantaneous, that is, $\Gamma_\mu(t) = 2\tau_\mu\delta(t)$, the collective dipole moment decays exponentially as

$$C_\mu(t) \propto \exp\left(-\frac{t}{\tau_\mu}\right) \quad (7)$$

in the diffusive time scale, that is, the time scale much slower than the decay of the angular velocity. Since the inertial motion decays within 0.1 ps in most liquids, it cannot be the reason of the non-exponential relaxation in the ps regime.

The dynamics of the total dipole moment of the system depends on the electrostatic boundary condition at the infinite distance due to the long-range nature of the Coulombic interaction. Accordingly, the relation between $C_\mu(t)$ and the frequency-dependent complex dielectric spectrum, $\epsilon(\omega)$, also depends on the electrostatic boundary condition. In the case of the conductive boundary condition, which is usually employed in MD simulation with the Ewald method for the Coulombic interaction, $\epsilon(\omega)$ is given in terms of $C_\mu(t)$ as[33]

$$\epsilon(\omega) - 1 = \frac{\langle|\boldsymbol{\mu}|^2\rangle}{3\epsilon_v k_B T V}\left[1 + i\omega\int_0^\infty dt e^{i\omega t} C_\mu(t)\right], \quad (8)$$

where ϵ_v, k_B, T, and V stand for the dielectric constant of vacuum, the Boltzmann constant, the absolute temperature, and the volume of the system, respectively, and ω denotes the angular frequency. The exponential decay as eq. (7) thus means the Debye relaxation in the frequency domain, and the deviation from the Debye function can be ascribed to the relaxation of the memory function in the finite time scale, which is related to the non-Markovian nature of the random force through eq. (3).

The purpose of this work is to relate the dynamics of the memory function to the relaxation of the liquid structure. As we have performed on shear viscosity, [30] we choose the two-body density as the descriptor of the liquid structure. The real-space description of the two-body density, $\rho_{\alpha\gamma}^{(2)}(\boldsymbol{r},t)$, is given by

$$\rho_\alpha(\boldsymbol{r},t) \equiv \sum_{i\in\alpha}\delta(\boldsymbol{r}-\boldsymbol{r}_i(t)), \tag{9}$$

$$\rho_{\alpha\gamma}^{(2)}(\boldsymbol{r},t) \equiv \frac{1}{V}\int d\boldsymbol{R}\,\rho_\alpha(\boldsymbol{r}+\boldsymbol{R},t)\rho_\gamma(\boldsymbol{R},t), \tag{10}$$

where α and γ are indices for the interaction sites. Its representation in the reciprocal space, $\tilde{\rho}_{\alpha\gamma}^{(2)}(\boldsymbol{q},t)$, is as follows:

$$\tilde{\rho}_\alpha(\boldsymbol{q},t) \equiv \int d\boldsymbol{r}\, e^{i\boldsymbol{q}\cdot\boldsymbol{r}}\rho_\alpha(\boldsymbol{r},t) = \sum_{i\in\alpha}e^{i\boldsymbol{q}\cdot\boldsymbol{r}_i(t)}, \tag{11}$$

$$\tilde{\rho}_{\alpha\gamma}^{(2)}(\boldsymbol{q},t) \equiv \frac{1}{V}\tilde{\rho}_\alpha(\boldsymbol{q},t)\tilde{\rho}_\gamma^{*}(\boldsymbol{q},t). \tag{12}$$

The real and reciprocal space representations are related with each other through the Fourier transformation. Their equilibrium averages are given by

$$\left\langle\rho_{\alpha\gamma}^{(2)}(\boldsymbol{r},t)\right\rangle = \rho_\alpha\omega_{\alpha\gamma}(|\boldsymbol{r}|) + \rho_\alpha\rho_\gamma g_{\alpha\gamma}(|\boldsymbol{r}|), \tag{13}$$

$$\left\langle\tilde{\rho}_{\alpha\gamma}^{(2)}(\boldsymbol{q},t)\right\rangle = \chi_{\alpha\gamma}(|\boldsymbol{q}|), \tag{14}$$

where ρ_α and ρ_γ are number densities of the sites α and γ, respectively. The functions $\omega_{\alpha\gamma}(|\boldsymbol{r}|)$, $g_{\alpha\gamma}(|\boldsymbol{r}|)$ and $\chi_{\alpha\gamma}(|\boldsymbol{q}|)$ denote the intramolecular correlation function, the site-site radial distribution function, and the partial structure factor, respectively. The latter two, $g_{\alpha\gamma}(|\boldsymbol{r}|)$ and $\chi_{\alpha\gamma}(|\boldsymbol{q}|)$, have traditionally been employed to describe equilibrium liquid structure. Therefore, the instantaneous values of $\rho_{\alpha\gamma}^{(2)}(\boldsymbol{r},t)$ and $\tilde{\rho}_{\alpha\gamma}^{(2)}(\boldsymbol{q},t)$ can be regarded as the measures of transient liquid structure.

In our previous work on shear viscosity, we demonstrated that the cross correlation function between the two-body density and the shear stress can describe the coupling

between the viscoelastic and the structural relaxations. [30] Since shear stress is actually the random force on the transverse momentum density in the low-q limit,[32] the corresponding function in the dielectric relaxation is the cross correlation function between $\boldsymbol{R}_{\mu}(t)$ and the two-body density as follows:

$$\rho^{(2)}_{\mu,\alpha\gamma}(\boldsymbol{r},t) \equiv \left\langle \rho^{(2)}_{\alpha\gamma}(\boldsymbol{r},0) R_{\mu,z}(t) \right\rangle, \tag{15}$$

$$\tilde{\rho}^{(2)}_{\mu,\alpha\gamma}(\boldsymbol{q},t) \equiv \left\langle \tilde{\rho}^{(2)}_{\alpha\gamma}(\boldsymbol{q},0) R_{\mu,z}(t) \right\rangle. \tag{16}$$

Consideration of the symmetry shows that the orientational dependence of $\rho^{(2)}_{\mu,\alpha\gamma}(\boldsymbol{r},t)$ and $\tilde{\rho}^{(2)}_{\mu,\alpha\gamma}(\boldsymbol{q},t)$ is p-type, that is, proportional to r_z/r and q_z/q, respectively. In particular, these two functions possess odd symmetry with respect to space inversion. On the other hand, according to their definitions, eqs. (11) and (12), the exchange of the site indices of $\rho^{(2)}_{\alpha\gamma}(\boldsymbol{r},t)$ and $\tilde{\rho}^{(2)}_{\alpha\gamma}(\boldsymbol{q},t)$ gives

$$\rho^{(2)}_{\gamma\alpha}(\boldsymbol{r},t) = \rho^{(2)}_{\alpha\gamma}(-\boldsymbol{r},t), \tag{17}$$

$$\tilde{\rho}^{(2)}_{\gamma\alpha}(\boldsymbol{q},t) = \tilde{\rho}^{(2)}_{\alpha\gamma}(-\boldsymbol{q},t). \tag{18}$$

Combination of them with the odd angular symmetry yields

$$\rho^{(2)}_{\mu,\gamma\alpha}(\boldsymbol{r},t) = -\rho^{(2)}_{\mu,\alpha\gamma}(\boldsymbol{r},t), \tag{19}$$

$$\tilde{\rho}^{(2)}_{\mu,\gamma\alpha}(\boldsymbol{q},t) = -\tilde{\rho}^{(2)}_{\mu,\alpha\gamma}(\boldsymbol{q},t). \tag{20}$$

As a result, the diagonal components, $\rho^{(2)}_{\mu,\alpha\alpha}(\boldsymbol{r},t)$ and $\tilde{\rho}^{(2)}_{\mu,\alpha\alpha}(\boldsymbol{q},t)$, vanish.

The substitution of eq. (1) into eqs. (15) and (16) gives

$$\begin{aligned} \rho^{(2)}_{\mu,\alpha\gamma}(\boldsymbol{r},t) &= \frac{1}{\Omega_0^2}\frac{\partial^2}{\partial t^2}\left\langle \rho^{(2)}_{\alpha\gamma}(\boldsymbol{r},0)\mu_z(t)\right\rangle \\ &+ \int_0^t d\tau \Gamma_{\mu}(t-\tau)\,\frac{\partial}{\partial\tau}\left\langle \rho^{(2)}_{\alpha\gamma}(\boldsymbol{r},0)\mu_z(\tau)\right\rangle + \left\langle \rho^{(2)}_{\alpha\gamma}(\boldsymbol{r},0)\mu_z(t)\right\rangle, \end{aligned} \tag{21}$$

$$\begin{aligned} \tilde{\rho}^{(2)}_{\mu,\alpha\gamma}(\boldsymbol{q},t) &= \frac{1}{\Omega_0^2}\frac{\partial^2}{\partial t^2}\left\langle \tilde{\rho}^{(2)}_{\alpha\gamma}(\boldsymbol{q},0)\mu_z(t)\right\rangle \\ &+ \int_0^t d\tau \Gamma_{\mu}(t-\tau)\,\frac{\partial}{\partial\tau}\left\langle \tilde{\rho}^{(2)}_{\alpha\gamma}(\boldsymbol{q},0)\mu_z(\tau)\right\rangle + \left\langle \tilde{\rho}^{(2)}_{\alpha\gamma}(\boldsymbol{q},0)\mu_z(t)\right\rangle. \end{aligned} \tag{22}$$

The cross correlation functions between the total dipole moment and the two-body density, $\langle \rho_{\alpha\gamma}^{(2)}(\boldsymbol{r},0)\mu_z(t)\rangle$ and $\langle \tilde{\rho}_{\alpha\gamma}^{(2)}(\boldsymbol{q},0)\mu_z(t)\rangle$, can be evaluated directly with MD simulation. Therefore, once $\Gamma_\mu(t)$ is obtained from $C_\mu(t)$, $\rho_{\mu,\alpha\gamma}^{(2)}(\boldsymbol{r},t)$ and $\tilde{\rho}_{\mu,\alpha\gamma}^{(2)}(\boldsymbol{q},t)$ can be calculated from the corresponding cross correlation functions using eqs. (21) and (22).

3. COMPUTATIONAL METHODS

The equilibrium MD simulation runs of liquid methanol and ethanol were performed using GROMACS 5.1.2 package.[34] In each system, 2744 molecules were contained in a cubic cell with periodic boundary condition. The temperature and the pressure of the system, 300 K and 1 bar, were controlled by the Nosé-Hoover thermostat and the Parrinello-Rahman barostat, respectively. [33] The time step was 1 fs, and the equation of motion was integrated with the leap-frog algorithm. [33] The production run of 100 ns was performed after the equilibration run of 10 ns length.

Both methanol and ethanol were described by the TraPPE-UA model, in which methyl (-CH_3) and methylene (-CH_2-) groups were treated as united atoms.[35] The Lorenz-Berthelot rule was applied to the Lennard-Jones (LJ) interaction between interaction sites of different kinds. [33] All the bond lengths were kept constant by LINCS algorithm. [36] The long-range Coulombic interaction was treated by means of particle mesh Ewald method with conductive boundary condition. The short-range parts of the Coulomb interaction and the LJ interaction were cut off at 1.4 nm distance.

The cross correlation functions, $\langle \rho_{\alpha\gamma}^{(2)}(\boldsymbol{r},0)\mu_z(t)\rangle$ and $\langle \tilde{\rho}_{\alpha\gamma}^{(2)}(\boldsymbol{q},0)\mu_z(t)\rangle$, were calculated independently in the real and the reciprocal spaces, respectively. The

corresponding functions for the shear stress were also evaluated in similar ways for comparison.

4. RESULTS AND DISCUSSION

4.1. Equilibrium liquid structure

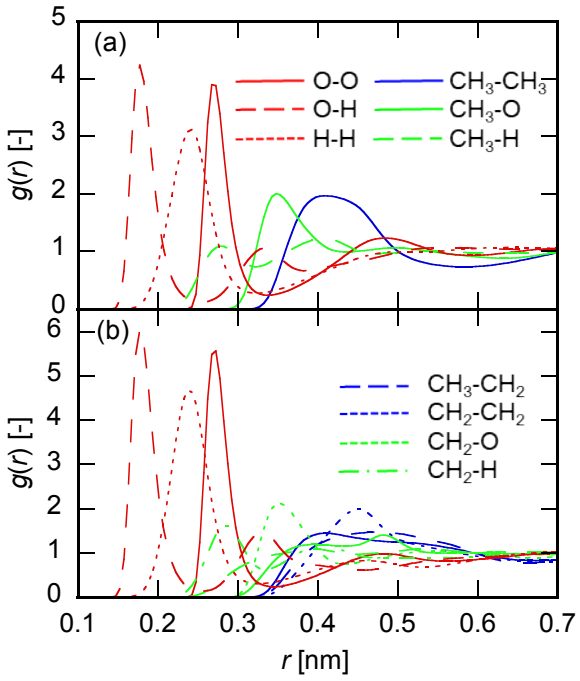

Figure 1. Site-site radial distribution functions of (a) liquid methanol and (b) ethanol. In (a), blue solid: CH_3-CH_3, green solid: CH_3-O, green dashed: CH_3-H, red solid: O-O, red dashed, O-H, red dotted: H-H. In (b), blue dashed: CH_3-CH_2, blue dotted: CH_2-CH_2, green dotted: CH_2-O, green dash-dotted: CH_2-H, and the meanings of other curves are the same as those in (a).

Before analyzing the coupling between the dielectric and structural relaxations, we show the liquid structures of methanol and ethanol in this subsection for reference.

The site-site radial distribution functions, $g(r)$, of both liquids are shown in Fig. 1. In Fig.1, $g(r)$ of OH-OH, OH-alkyl, and alkyl-alkyl components are plotted with red, green, and blue curves, respectively. The site-site radial distribution functions of both liquids are similar to each other. Their characteristic feature is the strong first peaks of the O-O, O-H, and H-H components, which describe a pair of sites directly connected with a hydrogen bond. The peak heights of ethanol are stronger than those of methanol because the number density of the former is lower than that of the latter.

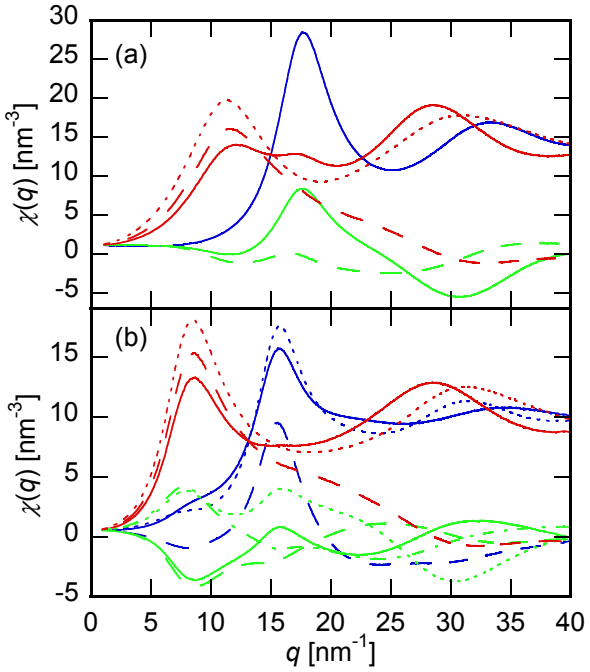

Figure 2. The partial structure factors of (a) methanol and (b) ethanol. The correspondence between the curves and the site-indices is the same as that of Fig. 1.

The partial structure factors in the reciprocal space are shown in Fig. 2. The prepeak structure is clearly observed at 12 nm^{-1} and 8 nm^{-1} for methanol and ethanol, respectively. The strongly positive correlation is found between OH groups at the prepeak in both liquids, which is consistent with previous works. [17, 30] The positive correlation between

the OH groups indicate that the prepeak originates in the aggregation of the OH groups through the hydrogen bond. A notable point on the prepeak is the correlations associated with the CH_2 group of ethanol. Its correlation with the CH_3 group is negative at the prepeak, while it exhibits positive correlations with both O and H atoms. It indicates that the CH_2 group belongs to the polar domain, rather than the nonpolar one, in the prepeak structure of ethanol.

The strong positive correlations between alkyl groups are observed at 18 nm^{-1} and 16 nm^{-1} in methanol and ethanol, respectively, which have been called "main peak". The main peak is thus assigned to the packing structure of alkyl groups within the nonpolar domain.

4.2. Dielectric relaxation

Inserting $\omega = 0$ into eq. (8), the static dielectric constant, $\epsilon(0)$, is given by

$$\epsilon(0) = \frac{\langle |\boldsymbol{\mu}|^2 \rangle}{3\epsilon_v k_B T V} + 1. \quad (23)$$

The values of the dielectric constants obtained in this study are 23.2 and 17.1 for methanol and ethanol, respectively, which is consistent with the values reported by previous MD simulation studies using the same molecular models. [5, 37] The dielectric constants are a little smaller than the experimental ones at 298 K, 32.7 for methanol and 24.6 for ethanol, [11] which should thus be ascribed to the insufficiency of the molecular model.

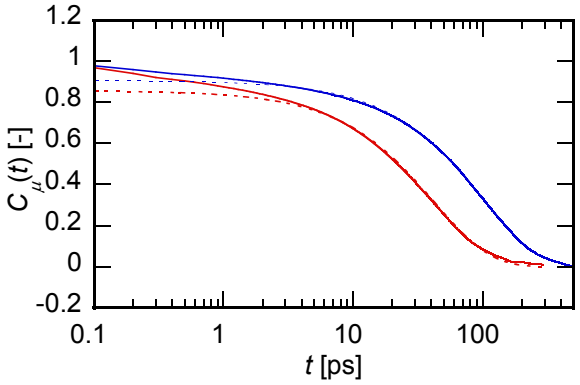

Figure 3. The normalized auto correlation functions of the collective dipole moment of methanol (red curve) and ethanol (blue curve). The simulation results and the exponential fittings are shown with solid and dotted curves, respectively.

The normalized time correlation functions of the total dipole moment, $C_\mu(t)$, are shown for both alcohols in Fig. 3. The fitting with an exponential function is also shown with the dotted curve. The slowest relaxation mode is approximated by an exponential function, whose time constant is 42 ps and 98 ps for methanol and ethanol, respectively, and the deviation from the exponential function is observed in the time scale faster than 10 ps. The slowest exponential mode corresponds to the principal Debye mode of the dielectric relaxation, and the deviation from the exponential function in the faster time scale is related to the high-frequency processes observed in experimental dielectric spectra. Our MD simulation thus describes the characteristic features of the dielectric relaxation of these two alcohols. The time constants of the slowest processes are a little smaller than the experimental one, 52 ps and 163 ps for methanol and ethanol, respectively. [3] We consider it is ascribed to the smaller static dielectric constant, because larger collective fluctuation leads to the slower relaxation. [9, 38]

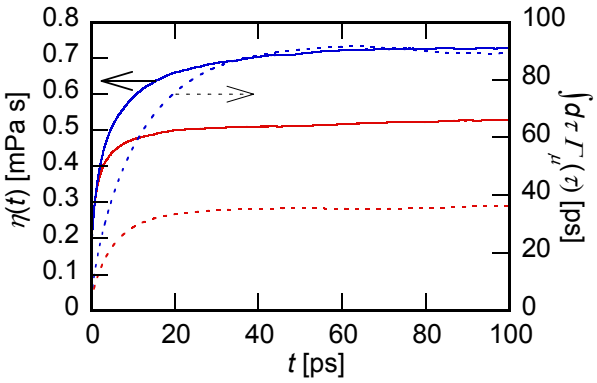

Figure 4. The running integrals of the time correlation function of shear stress (solid) and the memory function of the collective dipole moment (dotted). The functions for methanol and ethanol are plotted with red and blue curves, respectively.

The memory function of the collective dipole moment, $\Gamma_\mu(t)$, was calculated from the correlation function, $C_\mu(t)$, and its running integral is shown in Fig. 4 as the dotted curves. The convergence of the running integral, which is almost completed within 20 ps and 40 ps for methanol and ethanol, respectively, is faster than the decay of the correlation function shown in Fig. 3. The convergence of the memory function guarantees the exponential decay of $C_\mu(t)$ at longer time, and the decay of $\Gamma_\mu(t)$ in the finite time scale corresponds to the high-frequency processes of the dielectric spectrum.

According to the Kubo-Green theory, shear viscosity of liquid, η_0, is related to the time correlation function of the shear stress, P_{xy}, as

$$G(t) \equiv \frac{V}{k_B T}\langle P_{xy}(0)P_{xy}(t)\rangle, \tag{24}$$

$$\eta_0 = \int_0^\infty G(t)dt. \tag{25}$$

For comparison between the dielectric and viscoelastic relaxations, the running integral of the time correlation functions, defined as

$$\eta(t) \equiv \int_0^t G(\tau)d\tau, \tag{26}$$

is calculated and plotted in Fig. 4 together with the running integral of $\Gamma_\mu(t)$.

According to eqs. (25) and (26), the long-time limiting value of $\eta(t)$ is equal to the shear viscosity, η_0. The values of η_0 determined in this work are 0.53 mPa s (methanol) and 0.73 mPa s (ethanol). The value of methanol is close to the experiment, 0.55 mPa s, while that of ethanol is a little smaller than the experimental value, 1.08 mPa s. [11] The relative increase in η_0 from methanol to ethanol is smaller than the integrated dielectric relaxation time, τ_μ in eq. (6).

The time profile of $\eta(t)$ is composed of the fast stepwise rise at $t = 0$ and the slower rise. The fast stepwise component is ascribed to the collisional momentum transfer, and our previous work demonstrated that the dynamics of the heterogeneous structure contributes to the slow component in the case of methanol. [30] Fig. 4 shows that the larger viscosity of ethanol compared with methanol originates from the larger contribution of the slow component. Comparing the dynamics of the slow component of $\eta(t)$ with that of $\Gamma_\mu(t)$, the former appears a little faster. However, the time scales of these processes are close to each other, and we cannot judge, merely from the time profiles in Fig. 4, whether the microscopic origins of these processes are the same or not.

4.3. Coupling between dielectric and structural relaxations

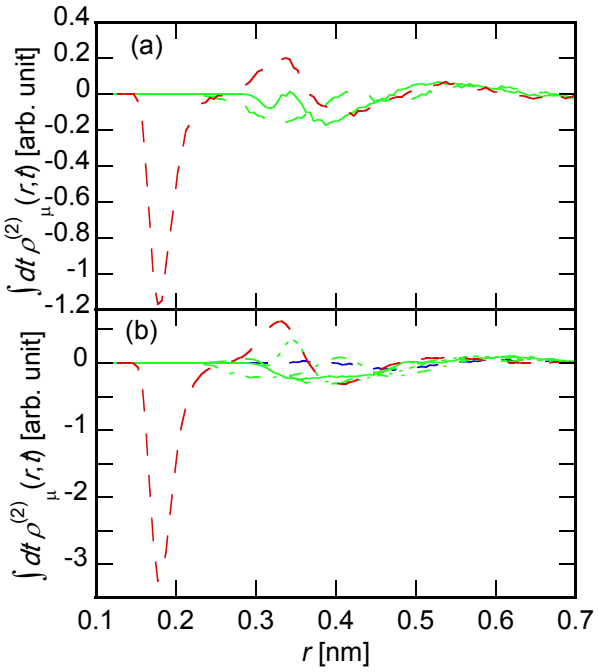

Figure 5. The cross correlation function between the random force on collective dipole moment and the two-body density in the real space, $\rho_{\mu,\alpha\gamma}^{(2)}(\boldsymbol{r},t)$, integrated over the time from t = 0 to 50 ps. The results on methanol and ethanol are shown in panels (a) and (b), respectively, and the correspondence between the curves and the site-indices is the same as that in Fig. 1. Only the off-diagonal components are plotted, because the diagonal ones vanish.

The cross correlation functions between the random force on collective dipole moment and the two-body density, $\rho_{\mu,\alpha\gamma}^{(2)}(\boldsymbol{r},t)$, are integrated over time to describe the coupling between the time-integrated friction and the liquid structure. The results on methanol and ethanol are shown in Figs. 5a and 5b, respectively. The upper limit of the time integral was chosen to be 50 ps for both liquids, because $\Gamma_{\mu}(t)$ plotted in Fig. 4 indicates that the memory is almost lost within 50 ps. Since diagonal components, $\rho_{\mu,\alpha\alpha}^{(2)}(\boldsymbol{r},t)$, are zero as was already described in Sec. 2, only the off-diagonal ones are shown in Fig. 5. The radial

dependence is shown in Fig. 5, omitting the trivial *p*-type angular dependence as was described in Sec. 2. In addition, the intramolecular part, where the sites α and γ belong to the same molecule, is subtracted in Fig. 5 for simplicity.

The profiles shown in Figs. 5a and 5b are similar to each other, suggesting that the mechanisms of the dielectric relaxations of both liquids are similar to each other. The most remarkable feature is the strong negative peak of the OH component at 0.18 nm, whose position is equal to the first peak of $g_{\mathrm{OH}}(r)$ shown in Fig. 1. The negative sign means that the collective dipole moment is likely to feel random force in the +*z* direction when oxygen atoms are subject to small number of hydrogen-bond donation from the +*z* direction. It is physically reasonable because an alcohol molecule can easily orient its H-atom toward +*z* direction when the H-atoms of other alcohol molecules are absent in the same direction.

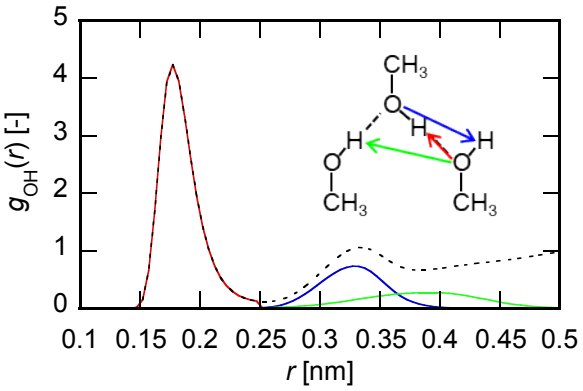

Figure 6. $g_{\mathrm{OH}}(r)$ of methanol (black dotted) is divided into the contributions of different configurations within a hydrogen-bonding chain. Red: direct hydrogen bond, Blue: the O-atom of the hydrogen-bond donor and the H-atom of the hydrogen-bond acceptor, Green: the O-atom of the partner of the H-donating hydrogen bond and the H-atom of the partner of the H-accepting hydrogen bond. These configurations are drawn as the cartoon in the inset with the arrows of the corresponding colors.

In addition to the strong negative peak at 0.18 nm, $\int_0^\infty \rho^{(2)}_{\mu,OH}(\boldsymbol{r},t)dt$ shows a positive peak at 0.33 nm and a negative one at 0.40 nm. In order to clarify the origins of these peaks, the static structure in this *r* region is analyzed in Fig. 6.

In Fig. 6, $g_{OH}(r)$ of methanol is divided into the contributions of different hydrogen-bond configurations. The red curve shows the direct hydrogen bond, the blue curve shows the pair of O- and H-atoms within a hydrogen-bonded pair of alcohol molecules that are not involved in the direct hydrogen bond, and the green curve shows the pair of the H-accepting O-atom and the H-donating H-atom of two different alcohol molecules connected to the same alcohol molecule through the hydrogen bonds. These configurations are drawn in the inset of Fig. 6 as the arrows of corresponding colors directed from the O- to the H-atoms. In this analysis, we employed a simple criterion of the hydrogen bond that the pair of O- and H-atoms within 0.25 nm, the first minimum of $g_{OH}(r)$, is regarded as bonded.

The peak position of the blue configuration, which is close to the second peak of $g_{OH}(r)$, corresponds to the positive peak of $\int_0^\infty \rho^{(2)}_{\mu,OH}(\boldsymbol{r},t)dt$ at 0.33 nm, while the green configuration forms a broad distribution around 0.40 nm, where the negative peak of $\int_0^\infty \rho^{(2)}_{\mu,OH}(\boldsymbol{r},t)dt$ exists. Therefore, we consider that the two peaks of $\int_0^\infty \rho^{(2)}_{\mu,OH}(\boldsymbol{r},t)dt$ exhibited in Fig. 5 can be assigned to the blue and green configurations within a hydrogen-bonding chain.

The linear hydrogen-bonding chain of a liquid alcohol is a directional chain. It should be noticed here that the direction of the blue arrow in Fig. 6 relative to the hydrogen-bonding chain is opposite to those of the red and green arrows. The difference in the direction corresponds to that of the sign of the peaks of $\int_0^\infty \rho^{(2)}_{\mu,OH}(\boldsymbol{r},t)dt$ in Fig. 5.

Therefore, the dynamic mode represented by $\int_0^\infty \rho^{(2)}_{\mu,OH}(\boldsymbol{r},t)dt$ in Fig. 5 is related to the inversion of the directional hydrogen-bonding chain.

In principle, the inversion of the chain occurs in two different ways. The first one is the collective rotation of the whole chain, and the second one is the alternating switching of hydrogen bonds within a chain. Since the dielectric relaxation shown in Fig. 3 represents the reorientation of the collective dipole moment, however, it seems unreasonable to consider that the rotation of the whole chain occurs faster than the dielectric relaxation. We therefore consider that $\int_0^\infty \rho^{(2)}_{\mu,OH}(\boldsymbol{r},t)dt$ in Fig. 5 is assigned to the alternating switching.

The picture of the dielectric relaxation of alcohols provided by our cross correlation analysis is consistent with the wait-and-switch model proposed for water and alcohols. [6, 7] In the wait-and-switch model, the reorientation of a dipole moment requires the rearrangement of the hydrogen-bonding network of the surrounding molecules to switch its hydrogen bond to a new partner. The integrated cross correlation function in this study, $\int_0^\infty \rho^{(2)}_{\mu,OH}(\boldsymbol{r},t)dt$, describes the collective fluctuation of the hydrogen-bonding network to accept the switching, and the high-frequency mode of the dielectric spectrum reveals the time scale of the fluctuation.

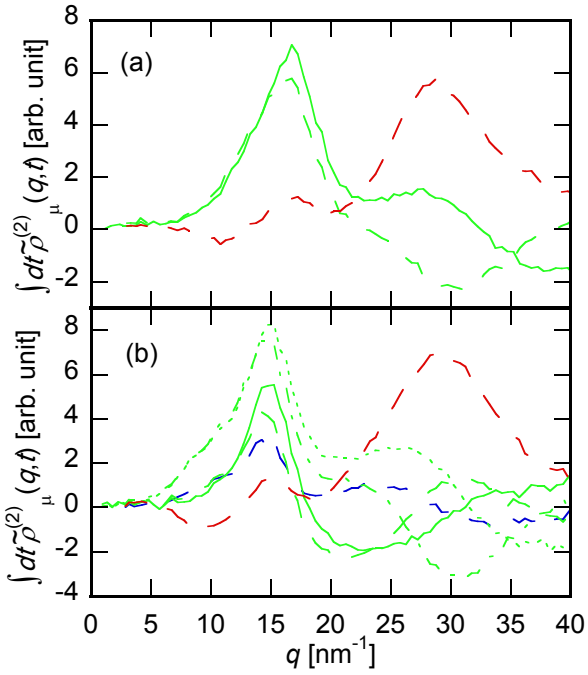

Figure 7. The cross correlation function between the random force on collective dipole moment and the two-body density in the reciprocal space, $\tilde{\rho}^{(2)}_{\mu,\alpha\gamma}(\boldsymbol{q},t)$, integrated over the time from $t = 0$ to 50 ps. The results on methanol and ethanol are shown in panels (a) and (b), respectively, and the correspondence between the curves and the site-indices is the same as that in Fig. 1. Only the off-diagonal components are plotted, because the diagonal ones vanish.

The reciprocal space representation of the time-integrated coupling, $\int_0^\infty \tilde{\rho}^{(2)}_{\mu,\alpha\gamma}(\boldsymbol{q},t)dt$, is shown in Fig. 7. The upper limit of the time integral is truncated at 50 ps, as is the case of the real-space counterpart in Fig. 5. The profiles of methanol and ethanol are similar to each other also in the reciprocal space. The trivial angular dependence is omitted as is the case of Fig. 5.

There are three important characteristics to be discussed in the profiles in Fig. 7. The first one is the large positive peak of the OH component around 30 nm^{-1}. The OH

correlation of the period of $2\pi / q \cong 0.2$ nm corresponds to the intrachain periodic structure of the linear hydrogen-bonding chain, and the period is also close to the distance between two negative peaks of $\int_0^\infty \rho^{(2)}_{\mu,OH}(\boldsymbol{r},t)dt$ in Fig. 5. We therefore call hereafter the structure around 30 nm^{-1} as "OH alternation mode".

The second characteristic point is the correlation at the main peak, 17 nm^{-1} for methanol and 15 nm^{-1} for ethanol. The main peak of the static structure factor, Fig. 2, represents the packing structure of the alkyl chain as was discussed in Sec. 4.1. Accordingly, the components involving the sites of the alkyl group exhibit strong correlation in Fig. 7. Therefore, the packing of the alkyl chain also contributes to the friction on the collective dipole moments of alcohols. An interesting point is that, in ethanol, the components associated with the CH_2 group show stronger correlation with those with the CH_3 group. This point will be discussed further in Sec. 4.5 in relation to the time profile of the cross correlation.

The third point is the weak coupling with the domain structure. At the positions of the prepeak, 12 nm^{-1} for methanol and 8 nm^{-1} for ethanol, a shallow basin is observed only in the OH component, and no structure is found in other components. It indicates that the relaxation of collective dipole moment is scarcely affected by the dynamics of the polar-nonpolar domain structure.

4.4. Stress-structure coupling

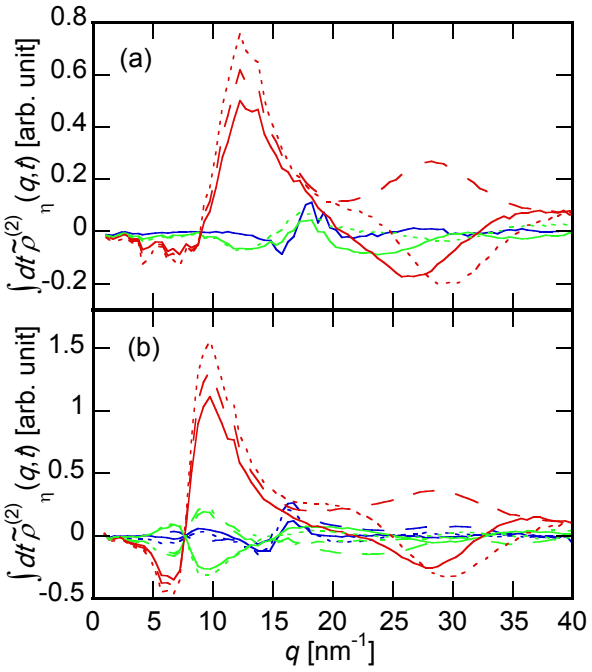

Figure 8. The time integral of the stress-structure coupling in the reciprocal space of (a) methanol and (b) ethanol. The correspondence between the curves and the site-indices is the same as that in Fig. 1.

For comparison between the dielectric and the viscoelastic relaxations, we show in Fig. 8 the cross correlation function between the shear stress and the two-body density defined in our previous work as[30]

$$\tilde{\rho}^{(2)}_{\eta,\alpha\gamma}(\boldsymbol{q},t) \equiv \left\langle \rho^{(2)}_{\alpha\gamma}(\boldsymbol{q},0) P_{xy}(t) \right\rangle. \tag{27}$$

The cross correlation functions are integrated over time as $\tilde{\rho}^{(2)}_{\mu,\alpha\gamma}(\boldsymbol{q},t)$ in Fig. 7. The d-type angular dependence of $\tilde{\rho}^{(2)}_{\eta,\alpha\gamma}(\boldsymbol{q},t)$, which is proportional to $q_x q_y/q^2$, is omitted in Fig. 8. Contrary to $\tilde{\rho}^{(2)}_{\mu,\alpha\gamma}(\boldsymbol{q},t)$, $\tilde{\rho}^{(2)}_{\eta,\alpha\gamma}(\boldsymbol{q},t)$ possesses even symmetry with respect to the permutation of α and γ as

$$\tilde{\rho}^{(2)}_{\eta,\alpha\gamma}(\boldsymbol{q},t) = \tilde{\rho}^{(2)}_{\eta,\gamma\alpha}(\boldsymbol{q},t). \tag{28}$$

Based on the linear response theory, $\frac{q^2}{q_x q_y}\int_0^\infty \tilde{\rho}^{(2)}_{\eta,\alpha\gamma}(\boldsymbol{q},t)dt$ describes the change in the structure factor under weak shear flow along the compression axis.

As we have already reported on methanol,[30] the shear stress shows strong coupling with the heterogeneous structure in both alcohols. The coupling at the prepeak is strong in the components associated with the OH group, as is the case of the partial static structure factors exhibited in Fig. 2. In these components, the correlation is strongly positive on the high-q side of the prepeak, and weakly negative correlation is also observed on the low-q side. The net positive correlation indicates that the hydrogen-bonding chain aligns along the extension axis in weak shear flow, and the derivative-shaped profile means that the distance between the different hydrogen-bonding chains is shortened along the compression axis. The negative correlation on the low-q side is weaker in methanol than in ethanol, which means that the shortening between hydrogen-bonding chains is not so remarkable in methanol. We consider it is because the alkyl domain of methanol has little room of compression due to its small volume fraction. Compared with the shear stress, the random force on the collective dipole moment shows little coupling with the heterogeneous structure as is demonstrated in Fig. 7, suggesting that the microscopic dynamics that gives the high-frequency processes of the dielectric relaxation is different from that of viscoelastic relaxation.

The coupling strength with the main peak is another difference between the dielectric and the viscoelastic relaxations. The strength of $\int_0^\infty \tilde{\rho}^{(2)}_{\eta,\alpha\gamma}(\boldsymbol{q},t)dt$ in Fig. 8 is small at the main peak, as we have already reported in our previous work. [30] On the other hand, $\int_0^\infty \tilde{\rho}^{(2)}_{\mu,\alpha\gamma}(\boldsymbol{q},t)dt$ shows large coupling at the main peak, as is shown in Fig. 7.

In addition to the coupling at the prepeak, the components related to the OH group also show strong coupling around the OH alternation mode. The diagonal OO and HH components show negative correlations, while the off-diagonal OH component is positive. It means that the alternating structure of O- and H-atoms within the hydrogen-bonding chain is strengthened along the extension axis of the shear flow, which is consistent with the alignment of the hydrogen-bonding chain suggested by the correlation at the prepeak.

4.5. Dynamics of coupling

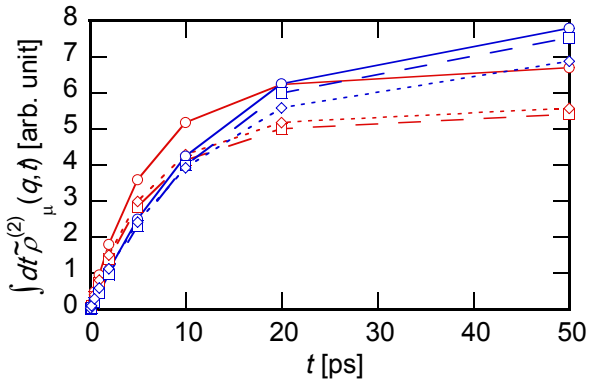

Figure 9. The running integrals of $\tilde{\rho}^{(2)}_{\mu,\alpha\gamma}(\boldsymbol{q},t)$ of methanol (red) and ethanol (blue). For methanol, solid: q = 17.3 nm^{-1}, CH_3-O, dashed: q = 17.3 nm^{-1}, CH_3-H, dotted: q = 29.2 nm^{-1}, OH. For ethanol, solid: q = 14.8 nm^{-1}, CH_2-O, dashed: q = 14.8 nm^{-1}, CH_2-H, dotted: q = 29.3 nm^{-1}, OH.

Figure 9 shows the running integral of the cross correlation function between the random force on collective dipole moment and the two-body density in the reciprocal space, $\int_0^t \tilde{\rho}^{(2)}_{\mu,\alpha\gamma}(\boldsymbol{q},\tau)d\tau$, at the characteristic structures. The solid lines show the CH_3-O (methanol) or CH_2-O (ethanol) correlation at the main peak, the dashed lines show the

CH_3-H (methanol) or CH_2-H (ethanol) correlation at the main peak, and the dotted line show the OH correlations at the OH alternation mode. These components are chosen because they exhibit strong coupling at the corresponding wavenumbers as is indicated in Fig. 7.

The convergence of the integral is slower for ethanol than for methanol, but the time profile hardly depends on the difference in the components or the values of q. In addition, the time profiles in Fig. 9 resemble the running integral of $\Gamma_\mu(t)$ of corresponding liquids shown in Fig. 4. The cross correlations at both the main peak and the OH alternation mode thus reflect a single dynamic mode, which gives both the high-frequency processes of the dielectric relaxation and the time-integrated friction on the collective dipole moment.

We would like to recall here that the coupling at the main peak is stronger for CH_2 than CH_3 sites in the case of ethanol. The structure around the CH_2 site is more likely to be affected by the motion of the OH group than the CH_3 one because the former is closer to the OH group. We thus consider that the coupling with the main peak is actually induced by the alternating switching of the hydrogen bonding. The reorientational motion of the OH group accompanies the motion of the adjacent CH_2 site, which perturbs the packing structure around the CH_2 site.

In our previous works on dynamics of water and aqueous solutions using mode-coupling theory (MCT), we demonstrated that the coupling between the charge- and polarity-density modes in low-q region gives dielectric friction on the reorientation of collective dipole moment. [39, 40] Since the prepeak is assigned to the contrast between the polar and nonpolar domains, the presence of the prepeak indicates the large fluctuation of the polarity density, which can be coupled to the charge-density mode to induce

dielectric friction based on the MCT expectation. However, such a coupling is hardly observed in the time-integrated cross correlation function, $\int_0^\infty \tilde{\rho}^{(2)}_{\mu,\alpha\gamma}(\boldsymbol{q},t)dt$, shown in Fig. 7.

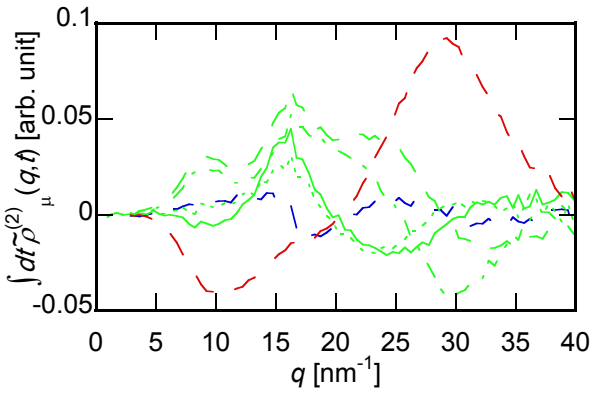

Figure 10. The cross correlation function of ethanol between the random force on collective dipole moment and the two-body density in the reciprocal space integrated from t = 0 to 0.15 ps. The correspondence between the curves and the site-indices is the same as that in Fig. 1.

In order to clarify the reason for the absence of the coupling with the prepeak in $\int_0^\infty \tilde{\rho}^{(2)}_{\mu,\alpha\gamma}(\boldsymbol{q},t)dt$, we calculated the time integral in the short time region by setting the upper limit of the time integral to be 0.15 ps. The result on ethanol is shown in Fig. 10. In contrast to the coupling integrated over the whole time in Fig. 7, the strong negative coupling of the OH component is clearly observed at the prepeak in the short-time integral shown in Fig. 10. Therefore, the instantaneous coupling between the random force and the prepeak is actually present as is expected from the analogy with the MCT analysis. However, the coupling is not reflected in the time-integrated profile, $\int_0^\infty \tilde{\rho}^{(2)}_{\mu,\alpha\gamma}(\boldsymbol{q},t)dt$, because the relaxation of the coupling is fast.

In MCT, the coupling between the charge- and the polarity-density modes occurs at the same wavevector $\boldsymbol{q}$. The fluctuation of the polarity density that gives the prepeak of alcohol is perpendicular to the hydrogen-bonding chain. The charge-density mode that couples to the polarity density must thus be perpendicular to the hydrogen-bonding chain, too.

The charge-density fluctuation of alcohols originates in the microscopic fluctuation of the orientation of the molecular dipole moment, a large part of which is assigned to that of the OH group. The fluctuation of the dipole moment within the hydrogen-bonding chain is anisotropic in both static and dynamic aspects. The fluctuation along the chain is expected to be large and slow, because it involves the alternating switching of the hydrogen bond. On the other hand, the fluctuation perpendicular to the chain is considered to be fast, because it can relax through the bending motion of the chain. Since the charge-density fluctuation coupled to the polarity mode is the latter, it cannot make large contribution to the time-integrated correlation with the random force on the collective dipole moment, $\int_0^\infty \tilde{\rho}^{(2)}_{\mu,\alpha\gamma}(\boldsymbol{q},t)dt$.

In MCT, the dynamics of the two-body density in the reciprocal space is approximated in terms of the product of partial intermediate scattering functions, $F_{\alpha\gamma}(q,t)$, defined as[32]

$$F_{\alpha\gamma}(|\boldsymbol{q}|,t) \equiv \frac{1}{V}\langle \rho^*_\alpha(\boldsymbol{q},0)\rho_\gamma(\boldsymbol{q},t)\rangle. \quad (29)$$

The approximation, usually called "factorization approximation", can be derived by regarding the fluctuation of the one-body density, $\rho_\alpha(\boldsymbol{q})$, as a Gaussian process. Based on the factorization approximation, we compared viscoelastic spectrum with the square of intermediate scattering function experimentally to judge whether the liquid structure at a given wavenumber can contribute to the shear viscosity. [27]

From the comparison between Figs. 7 and 8, it is noticed that the dielectric relaxation is coupled to the higher-q liquid structure than the viscoelastic relaxation. The relaxation of the intermediate scattering function tends to become faster with increasing q, because the decay of the higher-q mode requires motion of atoms of the smaller distance in the real space. Nonetheless, the viscoelastic relaxation is a little faster than that of the memory function for the collective dipole moment, as is exhibited in Fig. 4. It is thus necessary to examine whether the picture of the factorization approximation applies to the dynamics of the two-body density coupled to the dielectric relaxation.

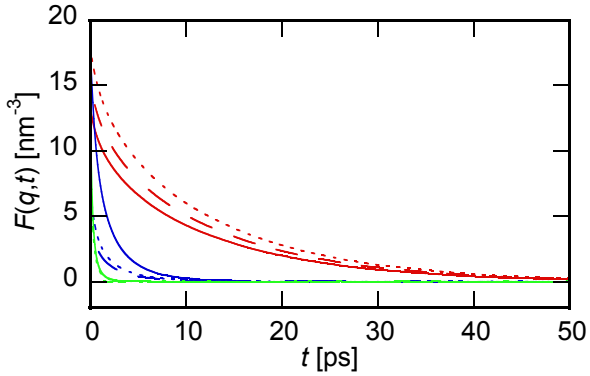

Figure 11. The partial intermediate scattering functions of ethanol at the prepeak (red, q = 8.8 nm^{-1}), main peak (blue, q = 15.6 nm^{-1}), and the OH alternation mode (green, q = 27.3 nm^{-1}). For prepeak, solid: O-O, dashed, O-H, and dotted: H-H. For main peak, solid: CH_2-CH_2, dashed, CH_2-O, and dotted: CH_2-H. For OH alternating mode, solid: O-O, dashed: O-H, and dotted: H-H.

Fig. 11 shows the partial intermediate scattering functions of ethanol at the wavenumbers of three characteristic structures. The components of the strong coupling with either viscoelastic or dielectric relaxations are plotted there. The relaxation of $F_{\alpha\gamma}(q,t)$ becomes faster with increasing q as expected. The relaxation at the prepeak occurs

in the time scale of 10 ps, which is consistent with the slow relaxation mode of $\eta(t)$ of ethanol in Fig. 4. On the other hand, since the relaxations at the main peak and the OH alternation mode are completed within 10 ps, the slow relaxation of the coupling at the corresponding wavenumber exhibited in Fig. 9 cannot be explained by the factorization approximation.

The factorization approximation is an approximation in which the motion of the two sites, α and γ, involved in $\tilde{\rho}^{(2)}_{\alpha\gamma}(\boldsymbol{q})$ are regarded to be independent of each other. In the case of the OH pair bound through a hydrogen bond, however, the O- and H-atoms are likely to diffuse together keeping the hydrogen bond between them. Such a motion can contribute to the decay of $F_{\alpha\gamma}(q,t)$, keeping $\tilde{\rho}^{(2)}_{OH}(\boldsymbol{q})$ unrelaxed. The breakdown of the factorization approximation may be understood also in terms of the central limiting theorem, which states that a stochastic process behaves as a Gaussian process when it consists of the contributions of many independent processes. Since a large number of molecules are involved in low-q mode, it is likely to behave as Gaussian, as is the case of the prepeak. On the other hand, the number of involved molecules is limited in the case of the OH alternation mode, which prevents the application of the central limiting theorem.

We have demonstrated so far in this work that the time-integrated coupling between the random force on the collective dipole moment and the two-body density at the prepeak is weak. We do not consider that the absence of the dynamic coupling means no influence of the heterogeneous structure to the dielectric relaxation of liquid alcohols. Rather, we guess that the dynamics of the OH alternation mode is affected by the heterogeneity of the structure in the static sense. The alternating switching of the hydrogen bond within a

chain is a collective dynamic mode, whose dynamics is affected by the strength of the static cooperativity. The strong prepeak indicates the large cooperativity of the chain, which will retard the relaxation time of the OH alternation mode.

4.6. Difference between dielectric and viscoelastic relaxations

The cross correlation analysis performed in this work demonstrated that the liquid structure coupled to the random force on the collective dipole moment of alcohols is the OH alternation mode around 30 nm^{-1}, together with the packing mode of the alkyl group. On the other hand, the shear stress is strongly correlated with the prepeak that represents the polar-nonpolar heterogeneous structure. Therefore, the microscopic dynamics that gives fast dielectric modes is different from that of the viscoelastic relaxation. Then, what makes the difference in the underling microscopic dynamics?

We consider that an important difference is that of symmetries. The collective dipole moment possesses *p*-type symmetry, while that of the shear stress is of *d*-type. The hydrogen-bonding chain of 1-alcohols is a directional chain, and its direction belongs to the *p*-type symmetry. The collective dipole moment is thus easily coupled to the dynamic mode that alters the direction of the chain, which is the alternating switching of the hydrogen bond. On the other hand, the distribution of the alkyl groups around the hydrogen-bonding chain possesses the *d*-type symmetry. Therefore, the shear stress is strongly coupled to the contrast between the OH and the alkyl groups represented as the prepeak. Although the prepeak may be coupled to the random force on the collective dipole moment through the combination with the polarization perpendicular to the hydrogen-bonding chain, it makes only small contribution to the time-integrated friction because its relaxation is fast.

The next question is whether the symmetry-based argument applies to other relaxation spectra of alcohols. In particular, the relation between the dielectric relaxation and depolarized light scattering spectra is quite interesting. Fukasawa and coworkers measured both the dielectric and the depolarized light scattering spectra of methanol in a wide frequency region.[4] From the comparison between these two spectra, they found that the slowest Debye mode of the dielectric spectrum is absent in the depolarized light scattering, but other high-frequency processes of the dielectric relaxation are observed in the light scattering spectrum, after dividing the time constants of the former by three to correct the difference in the reorientational relaxation times of the rank-1 (dipole) and the rank-2 (tensor) modes. [41] Based on the correspondence, they proposed that the dielectric and depolarized light scattering spectra observe the same dynamic modes except for the slowest Debye mode of the former. The comparison between the dielectric and depolarized light scattering spectra were performed on supercooled 1-propanol by Gabriel and coworkers. [13] They showed that the slowest mode of the former is absent in the latter, and that the other relaxation processes in the former, called α- and β-relaxations, are present also in the latter.

The spectrum of the depolarized light scattering is given by the time correlation function of the anisotropic part of the polarizability tensor,[41] which possesses the *d*-type symmetry as the shear stress tensor does. Therefore, the microscopic dynamics coupled to the depolarized light scattering is expected to be similar to the viscoelastic relaxation, and different from the dielectric relaxation, contrary to the experimental results described above. Our cross correlation analysis can also be applied to the polarizability tensor by calculating the cross correlation function between the anisotropic polarizability and the

two-body density. The random force on the polarizability can be correlated with the two-body density as well. Such an analysis is a plan of our future work.

5. SUMMARY

The cross correlation functions between the random force on the collective dipole moment and the two-body density were analyzed for liquid methanol and ethanol by MD simulation in order to extract the microscopic dynamic modes that govern the integrated dielectric relaxation time and the high-frequency dielectric modes. A strong coupling with the OH alternation mode around 30 nm^{-1} was found in both alcohols, which suggests that the coupling with the alternating switching mode of the hydrogen bond dominates the time-dependent friction on the collective dipole moment.

Contrary to the viscoelastic relaxation, the coupling with the two-body density at the prepeak is weak in the time-integrated cross correlation function, meaning that the dynamics of the heterogeneous structure little affect the integrated dielectric relaxation time. Although the coupling is present in the short-time region, it is not reflected in the integrated correlation, probably because the relaxation of the dipole moment perpendicular to the hydrogen-bonding chain is fast.

The difference in the symmetries of the shear stress and the collective dipole moment is proposed to be a possible reason for the difference in the microscopic modes coupled to their dynamics. The direction of the hydrogen-bonding chain is strongly coupled to the dielectric relaxation because of its *p*-type symmetry. On the other hand, the contrast between the OH and the alkyl groups is coupled to the shear stress due to its *d*-type symmetry around the hydrogen-bonding chain.

ACKNOWLEDGMENT

The author is grateful to the financial support by JSPS KAKENHI (Grant Number 19K03768).

REFERENCES

1. Böhmer, R.; Gainaru, C.; Richert, R., Structure and Dynamics of Monohydroxy Alcohols-Milestones towards Their Microscopic Understanding, 100 Years after Debye. *Phys. Rep.* **2014,** *545*, 125-195.

2. Bierwirth, S. P.; Bolle, J.; Bauer, S.; Sternemann, C.; Gainaru, C.; Tolan, M.; Böhmer, R., Scaling of Suprastructure and Dynamics in Pure and Mixed Debye Liquids. In *The Scaling of Relaxation Processes*; Kremer, F., Loidl, A., Eds.; Springer: Cham, 2018; pp 121-171.

3. Barthel, J.; Bachhuber, K.; Buchner, R.; Hetzenauer, H., Dielectric Spectra of Some Common Solvents in the Microwave Region. Water and Lower Alcohols. *Chem. Phys. Lett.* **1990,** *165*, 369-373.

4. Fukasawa, T.; Sato, T.; Watanabe, J.; Hama, Y.; Kunz, W.; Buchner, R., Relation between Dielectric and Low-Frequency Raman Spectra of Hydrogen-Bond Liquids. *Phys. Rev. Lett.* **2005,** *95*, 197802.

5. Cardona, J.; Sweatman, M. B.; Lue, L., Molecular Dynamics Investigation of the Influence of the Hydrogen Bond Networks in Ethanol/Water Mixtures on Dielectric Spectra. *J. Phys. Chem. B* **2018,** *122*, 1505-1515.

6. Kaatze, U.; Behrends, R.; Pottel, R., Hydrogen Network Fluctuations and Dielectric Spectrometry of Liquids. *J. Non·Cryst. Solids* **2002,** *305*, 19-28.

7. Sagal, M. W., Dielectric Relaxation in Liquid Alcohols and Diols. *J. Chem. Phys.* **1962,** *36*, 2437-2442.

8. Hansen, J.-P.; McDonald, I. R., *Theory of Simple Liquids*. 2nd ed.; Academic: London, 1986.

9. Madden, P.; Kivelson, D., A Consistent Molecular Treatment of Dielectric Phenomena. *Adv. Chem. Phys.* **2007,** *56*, 467-566.

10. Stoppa, A.; Nazet, A.; Buchner, R.; Thoman, A.; Walther, M., Dielectric Response and Collective Dynamics of Acetonitrile. *J. Mol. Liq.* **2015,** *212*, 963-968.

11. Riddich, J. A.; Bunger, W. B.; Sakano, T. K., *Organic Solvents*. 4th ed.; John Wiley & Sons: New York, 1986.

12. Davidson, D. W.; Cole, R. H., Dielectric Relaxation in Glycerol, Propylene Glycol, and n-Propanol. *J. Chem. Phys.* **1951,** *19*, 1484-1490.

13. Gabriel, J.; Pabst, F.; Blochowicz, T., Debye Process and beta-Relaxation in 1-Propanol Probed by Dielectric Spectroscopy and Depolarized Dynamic Light Scattering. *J. Phys. Chem. B* **2017,** *121*, 8847-8853.

14. Behrends, R.; Kaatze, U., Hydrogen Bonding and Chain Conformational Isomerization of Alcohols Probed by Ultrasonic Absorption and Shear Impedance Spectrometry. *J. Phys. Chem. A* **2001,** *105*, 5829-5835.

15. Kaatze, U.; Behrends, R., High-Frequency Shear Viscosity of Low-Viscosity Liquids. *Int. J. Thermophys.* **2014,** *35*, 2088-2106.

16. Jakobsen, B.; Maggi, C.; Christensen, T.; Dyre, J. C., Investigation of the Shear-Mechanical and Dielectric Relaxation Processes in Two Monoalcohols Close to the Glass Transition. *J. Chem. Phys.* **2008,** *129*, 184502.

17. Tomšič, M.; Bešter-Rogač, M.; Jamnik, A.; Kunz, W.; Touraud, D.; Bergmann, A.; Glatter, O., Nonionic Surfactant Brij 35 in Water and in Various Simple Alcohols: Structural Investigations by Small-Angle X-ray Scattering and Dynamic Light Scattering. *J. Phys. Chem. B* **2004,** *108*, 7021-7032.

18. Tomsic, M.; Jamnik, A.; Fritz-Popovski, G.; Glatter, O.; Vlcek, L., Structural Properties of Pure Simple Alcohols from Ethanol, Propanol, Butanol, Pentanol, to Hexanol: Comparing Monte Carlo Simulations with Experimental SAXS Data. *J. Phys. Chem. B* **2007,** *111*, 1738-1751.

19. Perera, A., Charge Ordering and Scattering Pre-Peaks in Ionic Liquids and Alcohols. *Phys. Chem. Chem. Phys.* **2017,** *19*, 1062-1073.

20. Canongia Lopes, J. N.; Padua, A. A., Nanostructural Organization in Ionic Liquids. *J. Phys. Chem. B* **2006,** *110*, 3330-3335.

21. Russina, O.; Triolo, A., New Experimental Evidence Supporting the Mesoscopic Segregation Model in Room Temperature Ionic Liquids. *Faraday Discuss.* **2012,** *154*, 97-109.

22. Kaur, S.; Gupta, A.; Kashyap, H. K., Nanoscale Spatial Heterogeneity in Deep Eutectic Solvents. *J. Phys. Chem. B* **2016,** *120*, 6712-6720.

23. Yamaguchi, T.; Yoshida, K.; Yamaguchi, T.; Kameda, Y.; Ikeda, K.; Otomo, T., Analysis of Prepeak Structure of Concentrated Organic Lithium Electrolyte by Means of Neutron Diffraction with Isotopic Substitution and Molecular Dynamics Simulation. *J. Phys. Chem. B* **2017,** *121*, 5355-5362.

24. Sillren, P.; Matic, A.; Karlsson, M.; Koza, M.; Maccarini, M.; Fouquet, P.; Gotz, M.; Bauer, T.; Gulich, R.; Lunkenheimer, P. et al., Liquid 1-Propanol Studied by Neutron Scattering, Near-Infrared, and Dielectric Spectroscopy. *J. Chem. Phys.* **2014,** *140*, 124501.

25. Bertrand, C. E.; Self, J. L.; Copley, J. R.; Faraone, A., Dynamic Signature of Molecular Association in Methanol. *J. Chem. Phys.* **2016,** *145*, 014502.

26. Bertrand, C. E.; Self, J. L.; Copley, J. R. D.; Faraone, A., Nanoscopic Length Scale Dependence of Hydrogen Bonded Molecular Associates' Dynamics in Methanol. *J. Chem. Phys.* **2017,** *146*, 194501.

27. Yamaguchi, T.; Saito, M.; Yoshida, K.; Yamaguchi, T.; Yoda, Y.; Seto, M., Structural Relaxation and Viscoelasticity of a Higher Alcohol with Mesoscopic Structure. *J. Phys. Chem. Lett.* **2018,** *9*, 298-301.

28. Yamaguchi, T.; Faraone, A.; Nagao, M., Collective Mesoscale Dynamics of Liquid 1-Dodecanol Studied by Neutron Spin-Echo Spectroscopy with Isotopic Substitution and Molecular Dynamics Simulation. *J. Phys. Chem. B* **2019,** *123*, 239-246.

29. Yamaguchi, T., Viscoelastic Relaxations of High Alcohols and Alkanes: Effects of Heterogeneous Structure and Translation-Orientation Coupling. *J. Chem. Phys.* **2017,** *146*, 094511.

30. Yamaguchi, T.; Faraone, A., Analysis of Shear Viscosity and Viscoelastic Relaxation of Liquid Methanol Based on Molecular Dynamics Simulation and Mode-Coupling Theory. *J. Chem. Phys.* **2017,** *146*, 244506.

31. Boon, J.-P.; Yip, S., *Molecular Hydrodynamics*. Dover: New York, 1991.

32. Balucani, U.; Zoppi, M., *Dynamics of the Liquid State*. Clarendon Press: Oxford, 1994.

33. Allen, M. P.; Tildesley, D. J., *Computer Simulation of Liquids*. Clarendon Press: Oxford, 1987.

34. Abraham, M. J.; Murtola, T.; Schulz, R.; Páll, S.; Smith, J. C.; Hess, B.; Lindahl, E., GROMACS: High Performance Molecular Simulations Through Multi-Level Parallelism from Laptops to Supercomputers. *SoftwareX* **2015,** *1-2*, 19-25.

35. Chen, B.; Potoff, J. J.; Siepmann, J. I., Monte Carlo Calculations for Alcohols and Their Mixtures with Alkanes. Transferable Potentials for Phase Equilibria. 5. United-Atom Description of Primary, Secondary, and Tertiary Alcohols. *J. Phys. Chem. B* **2001,** *105*, 3093-3104.

36. Hess, B.; Bekker, H.; Berendsen, H. J. C.; Fraaije, J. G. E. M., LINCS: A Linear Constraint Solver for Molecular Simulations. *J. Comput. Chem.* **1997,** *18*, 1463-1472.

37. Cruz Sanchez, M.; Dominguez, H.; Pizio, O. Molecular Dynamics Simulations of the Properties of Water-Methanol Mixtures. Effects of Force Fields. *Condens. Matter Phys.* **2019,** *22*, 1-14.

38. Yamaguchi, T.; Chong, S.-H.; Hirata, F., Dielectric Relaxation Spectrum of Water Studied by the Site-Site Generalized Langevin/Modified Mode-Coupling Theory. *Mol. Phys.* **2003,** *101*, 1211-1220.

39. Yamaguchi, T.; Chong, S.-H.; Hirata, F., Theoretical Study of the Molecular Motion of Liquid Water under High Pressure. *J. Chem. Phys.* **2003,** *119*, 1021-1034.

40. Yamaguchi, T.; Matsuoka, T.; Koda, S., Mode-Coupling Study on the Dynamics of Hydrophobic Hydration. *J. Chem. Phys.* **2004,** *120*, 7590-7601.

41. Rothschild, W. G., *Dynamics of Molecular Liquids*. John Wiley & Sons: New York, 1984.

TOC Graphic